


Nuclear deformation effects in the spectra of highly charged ions

Zewen Sun , Igor A. Valuev , and Natalia S. Oreshkina 

Max Planck Institute for Nuclear Physics, Saupfercheckweg 1, 69117 Heidelberg, Germany

 (Received 18 September 2023; revised 1 February 2024; accepted 23 May 2024; published 25 June 2024)

With the increasing precision of spectroscopic measurements, there is a growing demand for more accurate theoretical predictions, which requires the estimation of various higher-order effects, such as the nuclear deformation effect. Here, we present the results for nuclear deformation correction for the widest range of nuclei. The effects are investigated in terms of electronic transition energies, g factors, and hyperfine splitting constants, by implementing the deformed Fermi nuclear model to the Dirac equation. Based on the improved methodology and appropriate data classification, we present the results for over 1100 nuclei on figures, showing the general trends and anomalies. Moreover, it can serve as a simple tool providing estimations for specific planned research. In addition, we examine the connections and significance of deformation effects in the search of new physics with singly charged ions.

DOI: [10.1103/PhysRevResearch.6.023327](https://doi.org/10.1103/PhysRevResearch.6.023327)

I. INTRODUCTION

For highly charged ions (HCIs), the strong electron-nucleus interaction makes it an ideal probe to examine a variety of bound electron and nuclear properties, as well as providing a wide scope for fundamental theoretical [1–3] and experimental research [4–8]. Since the experimental precision is rapidly advancing [9], e.g., the measurements on transition energies [10–13] and g factor [14–20], there is a timely interest in the correspondingly accurate theoretical calculations. For such calculations, one should include not only the leading-order effect, but also various subleading atomic and nuclear contributions, e.g., few-loop quantum electrodynamic, nuclear deformation, and polarization effects. Among these, the nuclear deformation (ND) effect, arising from the distorted nuclear shapes, is one of the largest [21,22]. However, atomic theory predictions are almost exclusively based on a spherical model of nuclei. Therefore, when the required precision is high, or when the nuclear effects are expected to be sizable, it is important to understand to what extent the ND effects come into play for different observables and nuclei.

The inclusion of ND effects can also potentially change some atomic data, since the data determination requires combined efforts from experimental and theoretical sides, and theoretical models normally disregard ND effects. For example, the extraction of the relative change in root-mean-square (rms) radii from King's linearity has been commonly performed with significant simplifications of ND effects [23–25]. More recently, nonlinearity in the King plot garnered renewed research attention, aiming to search for new physics [26–28].

However, some mechanisms within the standard model (SM) can also create similar nonlinearities, e.g., ND effects [29] and a quadratic field shift [30]. Detailed investigations of ND effects can therefore illuminate the frontier of SM, and provide potential falsifiable evidence for the existence of the new physics as well as insights into the study of isotope shift.

In this paper, we focus on hydrogenlike HCIs and probe the ND effects for the widest possible range of nuclei by theoretical calculations on observables such as the binding and transition energies, g factor, and hyperfine splitting constant. Furthermore, the results can be proportionally generalized to more complex systems [31], since even for many-electron systems, the nuclear effects are almost exclusively determined by the interaction with innermost electrons. We employ an exact method to characterize the nuclear shape model by the rms charge radius and the intrinsic quadrupole moment Q_0 , and analyze the importance of nuclear shapes (prolate or oblate types). With the figures presenting the results for over 1100 HCIs, the general trend and some intriguing anomalies are easily visualizable, which hold value for future investigations. Finally, we discuss the ND contribution in the spectra of singly charged Yb^+ ions as a source of King's plot nonlinearities.

Relativistic units ($c = m_e = \hbar = \epsilon_0 = 1$) are used throughout the paper, unless explicitly given.

II. HAMILTONIAN WITH DEFORMED NUCLEI

The relativistic Hamiltonian obtained from Dirac equation is

$$H = \boldsymbol{\alpha} \cdot \mathbf{p} + \beta + V(r), \quad (1)$$

where $\boldsymbol{\alpha}$ and β are the Dirac matrices, and \mathbf{p} is the momentum operator of the electron, and the potential is defined as [32]

$$V(r) = -\frac{Z\alpha}{r} \left[\int_0^r r'^2 \rho(r') dr' + r \int_r^\infty r' \rho(r') dr' \right], \quad (2)$$

Published by the American Physical Society under the terms of the [Creative Commons Attribution 4.0 International license](https://creativecommons.org/licenses/by/4.0/). Further distribution of this work must maintain attribution to the author(s) and the published article's title, journal citation, and DOI. Open access publication funded by Max Planck Society.

TABLE I. Calculated deformed Fermi model parameters for selected nuclei, compared with literature values.

	a (fm)	R_{rms}^a (fm)	c^b (fm)	β_2^b	β_2^c
^{24}Mg	0.45855	3.0570(16)	3.0283	0.5604	0.6092(62)
^{40}Ca	0.52164	3.4776(19)	3.7132	0.1195	0.1196(44)
^{86}Sr	0.5234	4.2307(20)	4.82118	0.1490	0.1439(41)
^{132}Ba	0.5234	4.8303(47)	5.6533	0.1871	0.1844(62)
^{142}Nd	0.5234	4.9123(25)	5.8087	0.0958	0.0917(23)
^{168}Yb	0.5234	5.2702(56)	6.1485	0.3186	0.324(3)
^{238}U	0.5234	5.8521(33)	6.97678	0.2811	0.2741(36)

^aThe rms nuclear charge radii from Ref. [25].

^bNumerically calculated from Eqs. (4) and (5).

^cQuadrupole deformation parameters from Ref. [33].

where Z is the nuclear charge number, α is the fine-structure constant, and $\rho(r)$ is a spherical charge density.

In the general case of a nonspherical nucleus, the nuclear charge is described by the deformed Fermi distribution

$$\rho_{c\beta_2}(r, \theta) = \frac{\rho_0}{1 + \exp\left(\frac{r - c[1 + \beta_2 Y_2^0(\theta)]}{a}\right)}, \quad (3)$$

where c , β_2 , and a are the parameters for the model, Y_l^m denotes the spherical harmonics, and ρ_0 is the corresponding normalization factor. The spherically symmetric $\rho(r)$ in Eq. (2) can be obtained by averaging $\rho_{c\beta_2}(r, \theta)$ on the θ coordinate.

The nuclear charge distribution can be characterized by the rms nuclear charge radius R_{rms} and the intrinsic nuclear quadrupole moment Q_0 . Therefore, the parameters c and β_2 are determined such that R_{rms} and Q_0 calculated from $\rho_{c\beta_2}(r, \theta)$ match the tabulated nuclear data:

$$R_{\text{rms}}^2 = \int \rho_{c\beta_2}(r, \theta) r^2 d^3r, \quad (4)$$

$$Q_0 = Ze \int (3 \cos^2 \theta - 1) \rho_{c\beta_2}(r, \theta) r^2 d^3r. \quad (5)$$

The commonly adopted value for parameter a is 0.5234 fm [32]. It should be noted that for light nuclei, this value is comparable with their R_{rms} , which is clearly too large to deliver a reasonable description. Therefore, we artificially decrease the parameter as $a = 0.15R_{\text{rms}}$ for the cases when $R_{\text{rms}} < 3.5$ fm. When parameter a is determined, parameters c and β_2 can be numerically calculated using Eqs. (4) and (5).

Some examples of the calculated parameters and the comparison with existing values are tabulated in Table I. The comparison of our results with the corresponding β_2 from Ref. [33] shows overall good agreement. Since Ref. [33] uses a simplified analytic equation to calculate β_2 , whereas we use an exact numerical method, there are still small discrepancies, in particular for the light nuclei.

III. NUCLEAR DEFORMATION CORRECTIONS

In this paper, we investigate the ND effects in terms of transition energy $\delta E_{\text{tran,ND}}$, and g factor Δg_{ND} . By numerically solving the Dirac equation

$$H\Psi_{n\kappa m}(\mathbf{r}) = E_{n\kappa} \Psi_{n\kappa m}(\mathbf{r}), \quad (6)$$

we obtain the energies $E_{n\kappa}$ and the wave functions $\Psi_{n\kappa m}$, with

$$\Psi_{n\kappa m}(\mathbf{r}) = \frac{1}{r} \begin{pmatrix} G_{n\kappa}(r) \Omega_{\kappa m}(\theta, \varphi) \\ i F_{n\kappa}(r) \Omega_{-\kappa m}(\theta, \varphi) \end{pmatrix}, \quad (7)$$

where n is the principal quantum number, κ is the relativistic angular momentum number, and m is the total magnetic number.

The correction $\delta E_{\text{tran,ND}}$ is the relative difference between the transition energies of deformed $E_{\text{tran}}^{(c\beta_2)}$ and nondeformed $E_{\text{tran}}^{(c0)}$ Fermi nuclear models ($\beta_2 = 0$),

$$\delta E_{\text{tran,ND}} = \frac{E_{\text{tran}}^{(c\beta_2)} - E_{\text{tran}}^{(c0)}}{E_{\text{tran}}^{(c0)}}. \quad (8)$$

In our paper, we focus on the transition energy between $1s_{1/2}$ and $2p_{1/2}$ states.

The g factor is calculated theoretically from the radial wave functions,

$$g = \frac{2\kappa}{j(j+1)} \int_0^\infty G_{n\kappa}(r) F_{n\kappa}(r) r dr, \quad (9)$$

where $j = |\kappa| - 1/2$ is the total angular momentum number. The Δg_{ND} is the ND correction to the ground-state electron g factor, defined as

$$\Delta g_{\text{ND}} = g_{1s}^{(c\beta_2)} - g_{1s}^{(c0)}. \quad (10)$$

Additionally, the ND correction to the hyperfine splitting constant $\delta \mathcal{A}_{\text{ND}}$ is

$$\delta \mathcal{A}_{\text{ND}} = \frac{\mathcal{A}_{1s}^{(c\beta_2)} - \mathcal{A}_{1s}^{(c0)}}{\mathcal{A}_{1s}^{(c0)}}, \quad (11)$$

where \mathcal{A} is defined as

$$\mathcal{A} \propto \int_0^\infty G_{n\kappa}(r) F_{n\kappa}(r) \frac{1}{r^2} dr. \quad (12)$$

Here, we omit the angular prefactor, since this equation of proportionality is sufficient for the analysis.

Our calculations mainly consist of two parts. The first part is the calculation of parameters c and β_2 based on the experimentally measured ground-state nuclear rms radius and quadrupole moment. The radii R_{rms} are obtained from Ref. [25]. Additionally, when the data are not available, we

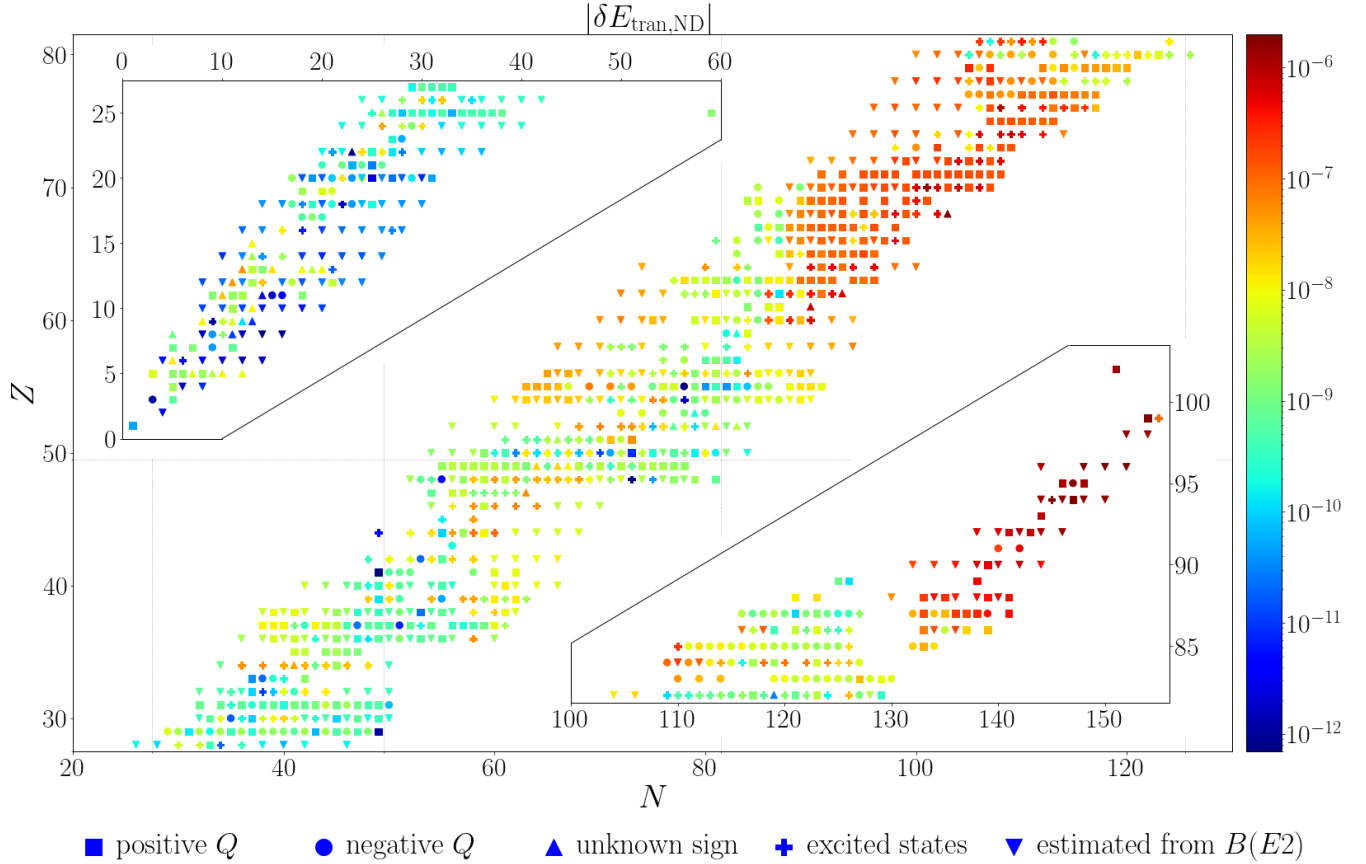


FIG. 1. Nuclear chart for ND correction $\delta E_{\text{tran,ND}}$ in $2p_{1/2} \rightarrow 1s_{1/2}$ transition energy. The gray grid lines refer to the magic numbers on the periodic table (20, 28, 50, 82, and 126). The marker styles indicate the properties of Q values used to calculate the ND correction, i.e., square: Q is positive; circle: Q is negative; up triangle: the sign of Q is unknown but we take it as positive; cross: Q obtained from a nuclear excited state instead of nuclear ground state; down triangle: Q_0 value is estimated from $B(E2) \uparrow$ transition rate (see more explanation in Sec. IV).

use the following empirical equation,

$$R_{\text{rms}} = \sqrt{\frac{3}{5}} R_0 = \sqrt{\frac{3}{5}} (1.2A^{1/3}) \text{ fm}, \quad (13)$$

where R_0 would correspond to the radius of a homogeneously charged sphere, and A is the nuclear mass number. The intrinsic quadrupole moment Q_0 values are retrieved from Refs. [33–35]. References [34,35] report the spectroscopic nuclear quadrupole moment Q , which is related to Q_0 via

$$Q_0 = \frac{(I+1)(2I+3)}{I(2I-1)} Q, \quad (14)$$

where I is the nuclear spin quantum number. Reference [33] provides adopted reduced quadrupole transition rates $B(E2) \uparrow$ for spinless nuclei from the nuclear ground state to the first excited 2^+ state, and Q_0 is obtained from

$$Q_0(b) = \sqrt{\frac{16\pi B(E2) \uparrow (e^2 b^2)}{5e^2}}. \quad (15)$$

As for the second part, we numerically solve Eq. (6) within the dual-kinetic-balance approach [36] and calculate the ND corrections defined by Eqs. (8) and (10).

IV. RESULTS AND DISCUSSION

As mentioned in Sec. III, the nuclear Q_0 data used to calculate ND corrections are taken from Refs. [33–35]. The Q values reported in Ref. [35] are experimentally measured by methods such as atomic spectroscopy, nuclear magnetic resonance, etc. Most of the Q values have well-defined signs indicating the shape of the corresponding nuclear charge distributions. If the sign is not determined, we assume it is positive, since positively deformed nuclei are the majority. In addition, some nuclei in Ref. [35] do not have Q data measured from the nuclear ground states (277 nuclei). The corresponding ND corrections are then calculated using the Q from the lowest available nuclear excited state. The Q_0 values obtained from the second data source [33] are calculated from experimentally measured $B(E2) \uparrow$ transition rates, using Eq. (15), which implicitly assume positive Q_0 . The data calculated from Q_0 with different signs and different references are separated on the plot by different marker styles (see Fig. 1).

In Figs. 1–3, we present the ND corrections for $\delta E_{\text{tran,ND}}$, Δg_{ND} , and δA_{ND} , respectively, for 1155 nuclei. The overall trend is that all three ND corrections are positively correlated with the Z number. However, some isotopes appear to be significantly different compared with their neighboring ones. For example, the nuclei on the shell closure feature smaller

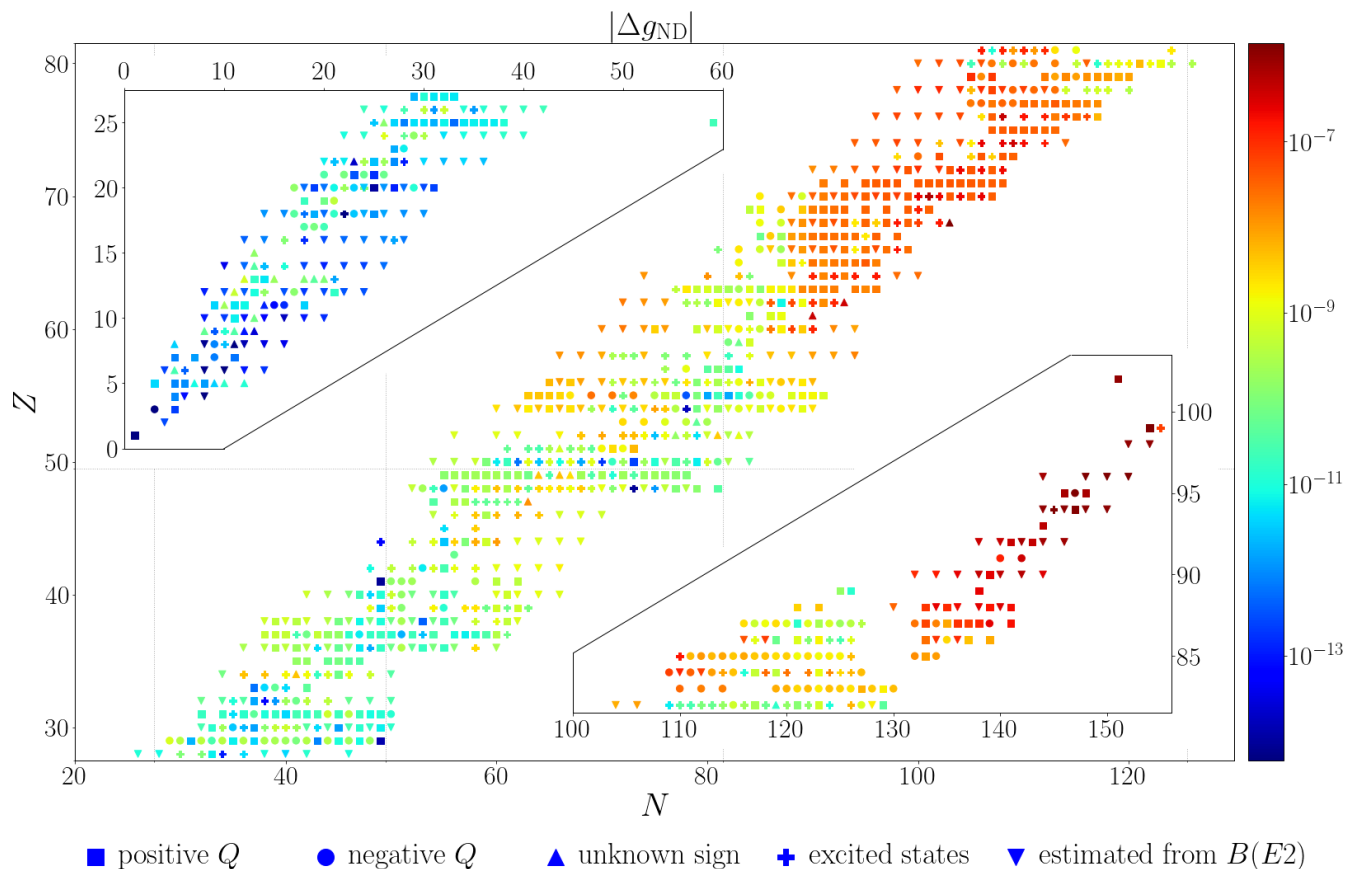


FIG. 2. Nuclear chart for the ND g -factor correction Δg_{ND} in the $1s$ state. See Fig. 1 for the legend.

deformations, whereas the edges of the isotope sequences are more likely to possess a higher degree of shape distortion and the corresponding ND effects. More importantly, for the nuclei with negative Q_0 values, the ND corrections are systematically higher up to three orders of magnitude than for other similar nuclei, highlighting the critical importance of the measured Q sign. Therefore, we conclude that the ND corrections based on the Q values with unspecified signs are less reliable.

There are tens of special nuclei in Ref. [35] that have either two measured Q values or two nuclear spins I , and correspondingly, two values of ND effects, whereas the figures only present the greater value. For some of these nuclei, the differences between the two values are not compatible, in particular, for the cases where the two Q values have opposite signs, i.e., ^{94}Mo , ^{96}Mo , ^{134}Ba , and ^{136}Ba .

For the spinless nuclei, the hyperfine splitting constants turn into zero, such that the ND corrections to it are not tangible. However, we keep the corresponding $\delta\mathcal{A}_{\text{ND}}$ data on Fig. 3, defined by Eq. (11) for the electronic part exclusively, for the sake of completeness and since the excited nuclear states can have nonzero spin. Although the ND effects appear to be significant for $\delta\mathcal{A}_{\text{ND}}$, for a relative change of $\sim 10^{-4}$ in heavy ions, it could be difficult to factorize this ND correction from the uncertainties of finite-nuclear-size and Bohr-Weisskopf effects [37].

The figures only show the results for the $1s$ electronic state or the $2p_{1/2} \rightarrow 1s_{1/2}$ transition, since the effect is maximized

at the ground states. For excited states, our estimations show that ND corrections lose up to one order of magnitude by every principal, orbital momentum, and total angular momentum quantum numbers.

Previous theoretical analyses [2,3] of the ND correction to the g factor were based on strictly positive Q_0 values calculated from $B(E2) \uparrow$ transition rates with Eq. (15). To avoid ambiguity in the sign of Q_0 we adopt the values in Ref. [35] instead, together with the measured signs, if available. This causes a slight discrepancy between our results and the corresponding data in Refs. [2,3], which can be removed by using the same β_2 as reported in Refs. [2,3].

We take ^{238}U , a highly deformed heavy isotope, as an example to perform an uncertainty analysis. For ^{238}U , the measured values and corresponding uncertainties are $R_{\text{rms}} = 5.8521(33)$ fm [25] and $Q_0 = 11.07(28)$ b [33]. We calculate the absolute ND energy correction for $1s$ state, $\Delta E_{1s,\text{ND}}$, at the vicinity of the measured R_{rms} and Q_0 values. For every 1% deviation of R_{rms} and Q_0 , the corresponding energy correction changes by 2.2% and 1.9%, respectively. However, since the measurement uncertainties of R_{rms} and Q_0 have every different magnitude, the relative uncertainty of energy correction is 0.1% and 5%, propagated from R_{rms} and Q_0 , respectively. It shows that the uncertainties mainly come from the measured quadrupole moment Q_0 , and the radius uncertainties are impactless. Since the measurement uncertainties for other isotopes do not differ by orders of magnitude, this conclusion can also be generalized to other isotopes.

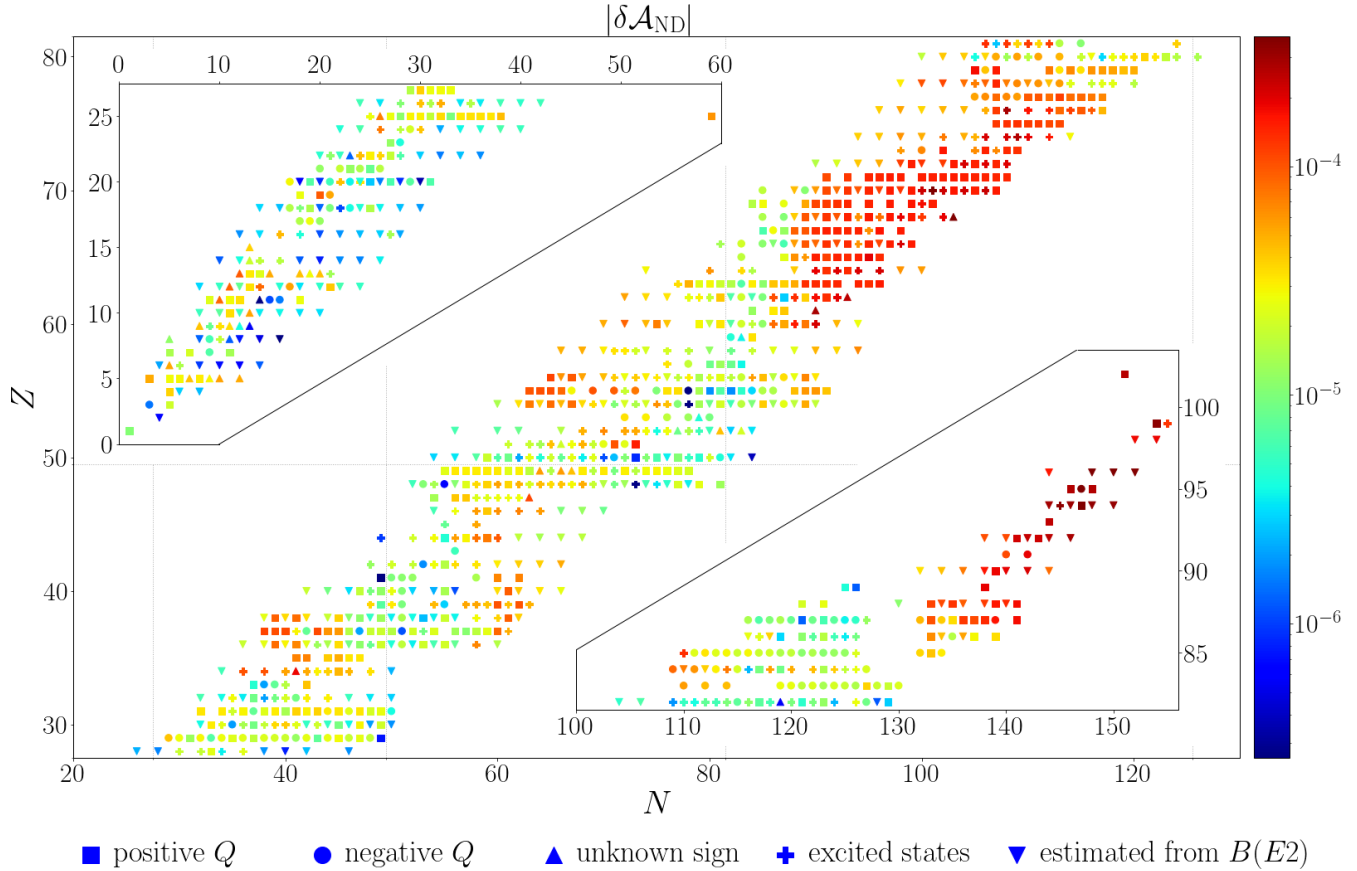


FIG. 3. Nuclear chart for the ND hyperfine splitting constant correction $\delta\mathcal{A}_{\text{ND}}$ in the $1s$ state. See Fig. 1 for the legend.

V. THE SEARCH FOR NEW PHYSICS

Recently, experimentally observed nonlinearity in the King plot of Yb^+ ions [28,30] led to a discussion on the existence of a new boson particle acting as a force carrier between electrons and neutrons. This is attributed to the observed nonlinearity being three times the experimental uncertainty, 3σ [30]. However, to claim the existence of new particles, one has to analyze nonlinearities from the existing physics, i.e., quadratic field shifts and ND effects [29,30].

The five isotopes $^{168,170,172,174,176}\text{Yb}^+$ and two transitions $6^2S_{1/2} \rightarrow 5^2D_{3/2}$, $5^2D_{5/2}$ have been chosen to generate the King plot [30]. Both transition energies have a measurement precision of ~ 300 Hz. To estimate the ND energy corrections, we use perturbation theory with a perturbing potential $\Delta V = V^{(c\beta_2)} - V^{(c0)}$, defined by Eqs. (2) and (3). The unperturbed many-electron wave functions of Yb^+ are calculated using the relativistic Hartree-Fock method, implemented with the GRASP2018 package [38]. Since both transitions involve only one valence electron, we use

$$\Delta E_{\text{diff,ND}}^A = \langle \Psi_{d3}^A | \Delta V | \Psi_{d3}^A \rangle - \langle \Psi_{d5}^A | \Delta V | \Psi_{d5}^A \rangle \quad (16)$$

to evaluate the ND correction to the difference between the two transition energies, where $|\Psi_{d3}^A\rangle$ and $|\Psi_{d5}^A\rangle$ are wave functions of the single valence electron in $5d_{3/2}$ and $5d_{5/2}$ configurations for isotope A . We would like to stress that

this is a simplified estimation, which fully ignores the core relaxation effects.

Unfortunately, the available Q values measured from nuclear ground states only cover $^{158,160,162,164,166,168}\text{Yb}^+$ isotopes [33]. Among these isotopes, our calculations predict the ND effect monotonically increases with the mass number A up to $\Delta E_{\text{diff,ND}}^{168} = 312$ Hz. The increase between isotopes ($\Delta E_{\text{diff,ND}}^{A+2} - \Delta E_{\text{diff,ND}}^A$) is ~ 30 – 50 Hz, which quantifies the King plot nonlinearity. Even though our results suggest that ND effects are not monotonic with respect to A in general (see Fig. 1), it is believed that the five observed [30] isotopes have the same nuclear ground state deformation $\beta_2 \approx 0.3$ [29] as $^{166,168}\text{Yb}^+$ examined above. Therefore we expect the ND contribution to the King plot nonlinearity to be at least on the same level of ~ 30 – 50 Hz. Summarizing, our estimation implies the ND effect alone is most probably not sufficient to explain the observed King plot nonlinearity [30]. However, it is well known that some underlying higher-order contributions can be a few orders of magnitude larger than the leading-order effect when highly localized potentials are involved [39–41]. In this case, it means that with the core relaxation effects included, the resulting ND effect can be significantly larger than the value obtained from Eq. (16). Further improvement requires knowledge of the nuclear quadrupole moments for the nuclei under consideration, more accurate calculations with fully correlated many-electron wave functions, and more realistic and sophisticated nuclear models.

VI. CONCLUSION

Based on the extensive analysis of available nuclear data, we present the most complete picture of ND corrections for different observables in hydrogenlike HCI. We provide pictures allowing order-of-magnitude estimations of the ND effects and the corresponding relevance for planned experiments. Although nuclei with higher Z numbers tend to be more deformed, the nuclear charts of ND corrections also show significant nonmonotonicity and case-by-case particularity. For example, the unstable nuclei at the edge of isotope sequences are normally more deformed than the stable ones, but some isotope sequences have the opposite features, e.g., Cu, Se, and In. Moreover, there are some individual outliers that appear to be significantly different from neighboring nuclei, e.g., ^{78}Cu , ^{90}Nb , ^{123}Sn , and $^{133,135,137}\text{Cs}$. If these are not

attributed to measurement deficiency, it leads to intriguing possibilities for future studies.

There is a noticeable portion of nuclei with negative Q_0 values that tend to have much higher deformation effects. We find that a sign flip in Q_0 can result in a difference of up to three orders of magnitude. This means that the ND contribution differs significantly for oblate and prolate types of nuclear deformation.

With our simple approach, we find that the nonlinearity observed from the King plot of singly charged ions cannot be adequately explained by the ND effects alone. However, since the required accuracy is high, reliable nuclear data, customized nuclear models, and more sophisticated atomic structure calculations are required to rule out ND effects completely as a source of the observed nonlinearity.

-
- [1] Y. S. Kozhedub, O. V. Andreev, V. M. Shabaev, I. I. Tupitsyn, C. Brandau, C. Kozhuharov, G. Plunien, and T. Stöhlker, Nuclear deformation effect on the binding energies in heavy ions, *Phys. Rev. A* **77**, 032501 (2008).
- [2] J. Zatorski, N. S. Oreshkina, C. H. Keitel, and Z. Harman, Nuclear shape effect on the g factor of hydrogenlike ions, *Phys. Rev. Lett.* **108**, 063005 (2012).
- [3] N. Michel, J. Zatorski, N. S. Oreshkina, and C. H. Keitel, Nonperturbative analysis of nuclear shape effects on the bound electron g factor, *Phys. Rev. A* **99**, 012505 (2019).
- [4] I. Draganić, J. R. Crespo López-Urrutia, R. DuBois, S. Fritzsche, V. M. Shabaev, R. S. Orts, I. I. Tupitsyn, Y. Zou, and J. Ullrich, High precision wavelength measurements of QED-sensitive forbidden transitions in highly charged argon ions, *Phys. Rev. Lett.* **91**, 183001 (2003).
- [5] A. Gumberidze, T. Stöhlker, D. Banaś, K. Beckert, P. Beller, H. F. Beyer, F. Bosch, S. Hagmann, C. Kozhuharov, D. Liesen *et al.*, Quantum electrodynamics in strong electric fields: The ground-state Lamb shift in hydrogenlike uranium, *Phys. Rev. Lett.* **94**, 223001 (2005).
- [6] J. Gunst, A. Surzhykov, A. Artemyev, S. Fritzsche, S. Tashenov, A. Maiorova, V. M. Shabaev, and T. Stöhlker, Parity-nonconservation effects on the radiative recombination of heavy hydrogenlike ions, *Phys. Rev. A* **87**, 032714 (2013).
- [7] H. Jörg, Z. Hu, H. Bekker, M. A. Blessenohl, D. Hollain, S. Fritzsche, A. Surzhykov, J. R. Crespo López-Urrutia, and S. Tashenov, Linear polarization of x-ray transitions due to dielectronic recombination in highly charged ions, *Phys. Rev. A* **91**, 042705 (2015).
- [8] J. Morgner, B. Tu, C. M. König, T. Sailer, F. Heiße, H. Bekker, B. Sikora, C. Lyu, V. A. Yerokhin, Z. Harman, J. R. Crespo López-Urrutia, C. H. Keitel, S. Sturm, and K. Blaum, Stringent test of QED with hydrogen-like tin, *Nature (London)* **622**, 53 (2023).
- [9] M. G. Kozlov, M. S. Safronova, J. R. Crespo López-Urrutia, and P. O. Schmidt, Highly charged ions: Optical clocks and applications in fundamental physics, *Rev. Mod. Phys.* **90**, 045005 (2018).
- [10] T. P. Heavner, E. A. Donley, F. Levi, G. Costanzo, T. E. Parker, J. H. Shirley, N. Ashby, S. Barlow, and S. R. Jefferts, First accuracy evaluation of NIST-F2, *Metrologia* **51**, 174 (2014).
- [11] F. Gebert, Y. Wan, F. Wolf, C. N. Angstmann, J. C. Berengut, and P. O. Schmidt, Precision isotope shift measurements in calcium ions using quantum logic detection schemes, *Phys. Rev. Lett.* **115**, 053003 (2015).
- [12] J. Ullmann, Z. Andelkovic, C. Brandau, A. Dax, W. Geithner, C. Geppert, C. Gorges, M. Hammen, V. Hannen, S. Kaufmann *et al.*, High precision hyperfine measurements in Bismuth challenge bound-state strong-field QED, *Nat. Commun.* **8**, 15484 (2017).
- [13] T. Leopold, S. A. King, P. Micke, A. Bautista-Salvador, J. C. Heip, C. Ospelkaus, J. R. Crespo López-Urrutia, and P. O. Schmidt, A cryogenic radio-frequency ion trap for quantum logic spectroscopy of highly charged ions, *Rev. Sci. Instrum.* **90**, 073201 (2019).
- [14] H. Häffner, T. Beier, N. Hermanspahn, H.-J. Kluge, W. Quint, S. Stahl, J. Verdú, and G. Werth, High-accuracy measurement of the magnetic moment anomaly of the electron bound in hydrogenlike carbon, *Phys. Rev. Lett.* **85**, 5308 (2000).
- [15] J. Verdú, S. Djekić, S. Stahl, T. Valenzuela, M. Vogel, G. Werth, T. Beier, H.-J. Kluge, and W. Quint, Electronic g factor of hydrogenlike oxygen $^{16}\text{O}^{7+}$, *Phys. Rev. Lett.* **92**, 093002 (2004).
- [16] B. Odom, D. Hanneke, B. D'Urso, and G. Gabrielse, New measurement of the electron magnetic moment using a one-electron quantum cyclotron, *Phys. Rev. Lett.* **97**, 030801 (2006).
- [17] S. Sturm, A. Wagner, B. Schabinger, J. Zatorski, Z. Harman, W. Quint, G. Werth, C. H. Keitel, and K. Blaum, g factor of hydrogenlike $^{28}\text{Si}^{13+}$, *Phys. Rev. Lett.* **107**, 023002 (2011).
- [18] I. Arapoglou, A. Egl, M. Höcker, T. Sailer, B. Tu, A. Weigel, R. Wolf, H. Cakir, V. A. Yerokhin, N. S. Oreshkina *et al.*, g factor of boronlike argon $^{40}\text{Ar}^{13+}$, *Phys. Rev. Lett.* **122**, 253001 (2019).
- [19] D. A. Glazov, F. Köhler-Langes, A. V. Volotka, K. Blaum, F. Heiße, G. Plunien, W. Quint, S. Rau, V. M. Shabaev, S. Sturm, and G. Werth, g factor of lithiumlike silicon: New challenge to bound-state QED, *Phys. Rev. Lett.* **123**, 173001 (2019).
- [20] F. Heiße, M. Door, T. Sailer, P. Filianin, J. Herkenhoff, C. M. König, K. Kromer, D. Lange, J. Morgner, A. Rischka,

- C. Schweiger, B. Tu, Y. N. Novikov, S. Eliseev, S. Sturm, and K. Blaum, High-precision determination of g factors and masses of $^{20}\text{Ne}^{9+}$ and $^{22}\text{Ne}^{9+}$, *Phys. Rev. Lett.* **131**, 253002 (2023).
- [21] V. Debierre, C. H. Keitel, and Z. Harman, Fifth-force search with the bound-electron g factor, *Phys. Lett. B* **807**, 135527 (2020).
- [22] V. Debierre, N. S. Oreshkina, I. A. Valuev, Z. Harman, and C. H. Keitel, Testing standard-model extensions with isotope shifts in few-electron ions, *Phys. Rev. A* **106**, 062801 (2022).
- [23] E. C. Seltzer, K x-ray isotope shifts, *Phys. Rev.* **188**, 1916 (1969).
- [24] G. Fricke, C. Bernhardt, K. Heilig, L. A. Schaller, L. Schellenberg, E. B. Shera, and C. W. DeJager, Nuclear ground state charge radii from electromagnetic interactions, *At. Data Nucl. Data Tables* **60**, 177 (1995).
- [25] I. Angeli and K. P. Marinova, Table of experimental nuclear ground state charge radii: An update, *At. Data Nucl. Data Tables* **99**, 69 (2013).
- [26] C. Delaunay, R. Ozeri, G. Perez, and Y. Soreq, Probing atomic Higgs-like forces at the precision frontier, *Phys. Rev. D* **96**, 093001 (2017).
- [27] J. C. Berengut, D. Budker, C. Delaunay, V. V. Flambaum, C. Frugiuele, E. Fuchs, C. Grojean, R. Harnik, R. Ozeri, G. Perez, and Y. Soreq, Probing new long-range interactions by isotope shift spectroscopy, *Phys. Rev. Lett.* **120**, 091801 (2018).
- [28] K. Ono, Y. Saito, T. Ishiyama, T. Higomoto, T. Takano, Y. Takasu, Y. Yamamoto, M. Tanaka, and Y. Takahashi, Observation of nonlinearity of generalized King plot in the search for new boson, *Phys. Rev. X* **12**, 021033 (2022).
- [29] S. O. Allehabi, V. A. Dzuba, V. V. Flambaum, and A. V. Afanasjev, Nuclear deformation as a source of the nonlinearity of the King plot in the Yb^+ ion, *Phys. Rev. A* **103**, L030801 (2021).
- [30] I. Counts, J. Hur, D. P. L. Aude Craik, H. Jeon, C. Leung, J. C. Berengut, A. Geddes, A. Kawasaki, W. Jhe, and V. Vuletić, Evidence for nonlinear isotope shift in Yb^+ search for new boson, *Phys. Rev. Lett.* **125**, 123002 (2020).
- [31] A. V. Viatkina, V. A. Yerokhin, and A. Surzhykov, Calculation of isotope shifts and King-plot nonlinearities in Ca^+ , *Phys. Rev. A* **108**, 022802 (2023).
- [32] F. A. Parpia and A. K. Mohanty, Relativistic basis-set calculations for atoms with Fermi nuclei, *Phys. Rev. A* **46**, 3735 (1992).
- [33] B. Pritychenko, M. Birch, B. Singh, and M. Horoi, Tables of E2 transition probabilities from the first 2^+ states in even-even nuclei, *At. Data Nucl. Data Tables* **107**, 1 (2016).
- [34] N. J. Stone, Table of nuclear electric quadrupole moments, *At. Data Nucl. Data Tables* **111-112**, 1 (2016).
- [35] N. J. Stone, *Table of Nuclear Electric Quadrupole Moments*, (IAEA, 2021).
- [36] V. M. Shabaev, I. I. Tupitsyn, V. A. Yerokhin, G. Plunien, and G. Soff, Dual kinetic balance approach to basis-set expansions for the Dirac equation, *Phys. Rev. Lett.* **93**, 130405 (2004).
- [37] V. M. Shabaev, O. V. Andreev, A. N. Artemyev, S. S. Baturin, A. A. Elizarov, Y. S. Kozhedub, N. S. Oreshkina, I. I. Tupitsyn, V. A. Yerokhin, and O. M. Zhrebtsov, QED effects in heavy few-electron ions, *Int. J. Mass Spectrom.* **251**, 109 (2006).
- [38] C. Froese Fischer, G. Gaigalas, P. Jönsson, and J. Bieroń, GRASP2018—A Fortran 95 version of the general relativistic atomic structure package, *Comput. Phys. Commun.* **237**, 184 (2019).
- [39] A. I. Bondarev, Y. S. Kozhedub, and N. S. Oreshkina, Finite nuclear size correction to vacuum polarization in hydrogen-like ions, *Opt. Spectrosc.* **109**, 823 (2010).
- [40] D. A. Glazov, A. V. Volotka, A. A. Schepetnov, M. M. Sokolov, V. M. Shabaev, I. I. Tupitsyn, and G. Plunien, g factor of boron-like ions: ground and excited states, *Phys. Scr.* **T156**, 014014 (2013).
- [41] V. Debierre and N. S. Oreshkina, Radiative and photon-exchange corrections to new-physics contributions to energy levels in few-electron ions, *Phys. Rev. A* **104**, 032825 (2021).